

THE EFFECT OF DIFFERENT ACCELERATORS ON THE CORROSION PROTECTION OF A SURFACE COATING ON SPHEROIDAL GRAPHITE CAST IRON (DUCTILE IRON)

BEÁTA HERBÁTH^{1*}, KRISTÓF KOVÁCS¹, MIKLÓS JAKAB¹

¹ Department of Materials Engineering, Faculty of Engineering, University of Pannonia, P.O. Box 1158, Veszprém, H-8201, HUNGARY

This study investigates the structure and composition of the zinc phosphate coating formed on the surface of nodular cast iron as well as the corrosion resistance of the electrophoretic paint applied to the conversion layers when nitrite-based and nitroguanidine accelerators are used. In the case of different accelerators, the structure of the zinc phosphate layer that forms when exposed to low, normal and high dosages was examined. This type of casting, in addition to steel casting, is commonly used in the production of agricultural vehicles due to its favorable mechanical properties. Although the majority of studies have summarized its application in the automotive industry by focusing on the phosphating of steel, galvanized steel and aluminum-based alloys, on complex vehicle assembly lines, cast iron is also used in phosphating processes that occur simultaneously. During our investigation into the use of different accelerators, a different crystal structure formed on the surface of the cast iron but did not affect the corrosion resistance of the electrophoretic painted samples.

Keywords: zinc phosphate, accelerator, spheroidal graphite cast iron, cathodic electrodeposition, corrosion resistance

1. Introduction

Zinc phosphate coatings on metal surfaces are very often the first layers of multilayer corrosion protection coatings, which are expected to form a hard, uniform, non-conductive surface coating on the surface of a base metal. These layers adhere tightly to the metal surface, thereby protecting the base metal from the effects of corrosion in the event of damage to the corrosion protection coating and ensuring the applied paint layer adheres properly, because the specific size of the surfaces covered with phosphate crystals is five to six times larger compared to that of the untreated metal surfaces. Phosphate treatments are usually applied to carbon steel, cast iron, low-alloy steel, galvanized and hot-dip galvanized steel, as well as aluminum and magnesium alloys, moreover, the zinc phosphate crystals are formed during a chemical conversion process. An important development of zinc phosphate baths was the modern tri-cationic conversion coating bath containing Zn^{2+} , Mn^{2+} and Ni^{2+} , which is suitable for depositing an excellent, highly resistant phosphate coating on multi-metal structures used in vehicle manufacturing, especially for outdoor use in corrosive environments. These coatings are highly suitable in cathodic electrophoretic paints due to their excellent surface properties [1]-[5].

Influence of the nature of the substrate on coating properties.

The difference between the zinc phosphate coating created on the surface of steel and nodular cast iron depends on the alloying elements and surface roughness. Phosphatability is promoted by small amounts of elements such as nickel, chromium and vanadium in the alloy, however, if the concentration of these elements exceeds a certain limit, the formation of the coating will be somewhat inhibited. The amount of carbon, phosphorus, sulfur, manganese and silicon can greatly influence the phosphatability of steel. Low carbon steels can be easily phosphated, resulting in high-quality surface coatings. Nevertheless, by increasing the carbon content, the rate of phosphating decreases and the crystals become larger.

A higher surface roughness increases the weight of the coating as well as its fineness and shortens the phosphating reaction time, thereby improving its structure and texture, whereas polished surfaces react poorly to phosphating. The explanation for this is that if a larger number of peaks and grooves are found on the metal surface, the effectiveness of the pickling reaction during phosphating increases due to the larger specific surface area, which also results in a good degree of adhesion of the coating. Although the phosphatability can be improved by increasing the surface roughness [6]-[7], in the case of electrophoretic painting, the weight of the

coating must be kept within strict tolerance limits since the phosphate layer insulates the base metal and a conductive surface is necessary for electrophoretic painting.

This study investigates zinc phosphating of nodular cast iron surfaces on the same technological line using the same parameters as well as nitrite-based (N) and nitroguanidine (NG) accelerators. Even though nitrite-based accelerators are the most commonly used and most effective for steel surfaces, the disadvantage of these systems is that the nitrite concentration usually must remain high, especially for spraying processes, thereby polluting the effluent and producing toxic nitrous gases. Organic nitrogen compounds, e.g. nitroguanidine, are used to reduce or eliminate the effects of the nitrous gases generated when using nitrite-based accelerators, especially in low-zinc baths, resulting in a softer and easily removable sludge. The disadvantage of nitroguanidine accelerators is that they have to be used at relatively high concentrations, moreover, can only be controlled to a sufficient level of accuracy by conducting a complex analysis in the phosphate solution and be dosed as precisely as possible in the ratio of the phosphating agent. One advantage of them is that they do not decompose spontaneously and can be used over a very wide dosage range, allowing robust processes to be developed [2,6-7]. The phosphating bath can be modified, e.g. by adding Na_2MoO_4 in the case of cast iron, since the presence of molybdenum in the coating can improve the adhesion of paint to the surface of the casting [8].

The main materials used for making car or vehicle parts and components are steel, aluminum, magnesium, copper, plastics and carbon fiber. Lightweight materials such as aluminum or magnesium are increasingly being used in the automotive industry in order to replace steel and iron components. Steel has been the dominant material since the 1920s and still remains the primary construction material for automotive bodies. However, the trend of reducing the weight of car bodies to minimize carbon emissions has gradually decreased the use of steel and cast iron. The lightweight nature of vehicles composed of aluminum would reduce fuel consumption but increase pollution resulting from the production of materials relative to those required for a conventional vehicle. Iron and steel are the critical elements in the structure of the vast majority of vehicles because they are low-cost [9]-[11]. In recent years, pretreatment processes have been modified not only to accommodate a wide variety of substrates but also to comply with environmental regulations and economic considerations [10].

Material substitution is often used to reduce the mass of vehicles. Low-carbon steel and iron have been replaced by lighter materials such as aluminum, high-strength steel and plastics. However, the impacts associated with the production of aluminum are more significant than those concerning heavier metals such as iron and steel, a common trade-off for lightweight materials. In comparison to iron, it has poorer mechanical properties (e.g. strength, stiffness, high temperature

performance and damping capacity) and higher production costs [12].

The wall thickness of thin wall ductile iron (TWDI) with a ferritic-pearlitic matrix or thin wall austempered ductile iron (TWADI) with an ausferritic matrix is 3 mm or less, both of which can be significant ferrous alloys to replace the current aluminum alloy parts that have traditionally been cast in ferrous alloys over a diverse range of applications, particularly those with high mechanical requirements, bringing about substantial savings. Lightweight nodular iron castings can be loaded to similar TWDI or higher TWADI working conditions as those the forged aluminum alloy was exposed to without suffering any potential failures [13]-[14].

The decision to substitute cast iron with aluminum alloys, and vice versa, is not always rational and must be preceded by a thorough analysis of all the factors involved such as mechanical properties at room and elevated temperatures, wear and material compatibility with parts made of different materials (galvanic corrosion), damping and noise, total energy consumption, as well as production costs [13]. Although cast iron inherently hardens surfaces, this is not the case with Al or Mg alloys that are not subjected to additional expensive processing. The relatively low damping capacity of Al alloys compared to cast iron generally results in significant engine or gearbox noise. In order to reduce such noise, various methods are implementable, however, all of them increase costs and engine weight. The manufacture of cast iron is related to energy savings when compared to aluminum alloys due to the high energy requirement of electrolysis during aluminum production. The cast iron can be remelted as many times as is necessary without its quality deteriorating and its production costs are lower when compared with aluminum alloys.

In addition to car production, transportation and agricultural vehicle production has developed significantly with material substitution being used to achieve mass reduction in vehicles such as trucks, tractors and harvesters. However, due to high demand in these sectors, in addition to steel and aluminum castings, iron castings, especially spheroidal iron castings, still play a major role. Reducing the thickness of cast iron, referred to as thin-walling, has the potential to enable cast iron to compete with cast aluminum in terms of weight while retaining its superior mechanical properties [15]. Lightweight truck-trailers contain wheel hubs and suspensions of austempered ductile iron (ADI) due to the following advantages: strength-to-weight ratio, stiffness, noise, cost and recyclability [16].

In addition to the mechanical tests conducted on nodular cast irons, the characteristics that by and large determine the properties of the raw material (yield strength, tensile strength, elongation, Brinell hardness, wear resistance) are examined after appropriate surface preparation (grinding, polishing, sample embedding, etching). The size, form and morphology of carbon-based particles as well as the ferrite and pearlite content are usually investigated by light microscopy [17]-[20]. Since adhesion of the conversion layer during the zinc

phosphating process carried out on ductile iron may be weaker in the case of larger graphite nodules on the surface than on the adjacent surfaces, it is also important to examine its microstructure [21]. Although sufficient dispersion of fine carbon particles in the phosphating bath can improve the degree of corrosion protection [22], this effect cannot be achieved by including graphite particles in the matrix.

Surface cleaning before chemical surface pretreatment

Abrasive blast cleaning of cast iron can completely remove rust and mill scale, resulting in a uniform surface light grey in color in the absence of shadows or spots of rust. However, varying degrees of surface cleanliness can be achieved by this method. Metallic abrasives such as steel or iron shot and grit as well as wire are widely used. Given that surface blasting using steel grit yielded a good level of surface cleanliness, the coating that was subsequently applied resulted in a satisfactory degree of adhesion due to the creation of highly irregular surfaces. This is important for optimal anchoring of the coating and its adhesion.

Phosphate crystals are electrical insulators but contain pores on approximately 1 % of their surface. This is a very important prerequisite for the deposition of an electrocoating.

The typical compositions of the conversion layers on steel, zinc, iron and aluminum substrates are varied in nature. The microstructures of the zinc phosphate coatings on steel, cast iron, zinc and aluminum surfaces are different. Although their morphology depends on the type of substrate used, the results in terms of adhesion of the electrocoat primer are similar [23].

Electrocoat

Electrocoat paints are aqueous dispersions consisting of typical paint ingredients such as film-forming agents (resins), pigments, extenders, additives and some solvents. These positively charged paints are suitable for use in coatings applied by cathodic electrodeposition (CED). For components in the automotive industry and now also in vehicle manufacturing, nowadays CED coatings predominantly achieve the best degree of corrosion protection [24].

Corrosion testing methods

Corrosion testing methods can simulate the degradation of coatings and paints in a corrosive cabinet by continuously and strictly controlling the humidity, temperature and concentration of salts. The Natural Salt Spray test (NSS) according to ISO 9227 is used to test the corrosion resistance of corrosion protection coatings applied to steel surfaces [25].

The effectiveness of phosphate coatings is evaluated by determining the spread of rust from scratches or other forms of surface damage to the paint film from the results of the Natural Salt Spray tests. This test is particularly important because vehicles are often exposed to moisture as well as the salt used to de-ice and

remove frost from road surfaces as described by Benchaldi et al., who examined the corrosion susceptibility of steels in a perchloric acid environment [26]-[27].

The aim of this study was to examine whether special attention should be paid to the surface pretreatment of cast-iron components during the design of corrosion protection coatings or if they can be pretreated in the same way as steel as is the case with complex workpieces from the automotive industry that contain different base metals.

2. Experimental

2.1. Samples and Measurements

2.1.1. Materials

Ductile iron (spheroidal or nodular) materials are very strong, flexible, durable and elastic in nature due to their unique microstructure. Ductile cast iron normally consists of at least 3 percent carbon and its free graphite particles are present as tiny spheres (nodules). Its mechanical properties are similar to those of steel and far superior to those of standard forms of cast iron. The tensile strength of ductile iron is excellent and is more resistant to tension than other forms of cast iron, so ductile cast iron does not break easily on impact [28].

Casting process of the sample plates

The samples used in the experiments were cast iron plates (*Figure 1*) according to EN-GJS-450-10 (5.3107) iron grade "Standard BS EN 1563:2011 Spheroidal graphite cast iron" produced by following the same method and technology as employed when manufacturing wheel hubs. Cast plates can be used to successfully simulate changes that occur on the original parts, making them easier to handle during experiments.

The test plates were manufactured according to the following process. A crucible-type induction furnace with a capacity of 8 tons was used to melt the metals. The charge consisted of crude iron, scrap steel and carbonizing materials. The composition and temperature of the base iron was checked with a spectrometer and pyrometer, respectively. The melt was transferred into a channel-type induction furnace with a capacity of 60 tons, where the base iron was homogenized. The treatment was carried out using the tundish cover method [29]. The treatment vessel was transferred to the molding line, where the slag was removed and then suitable examples of coins were taken from the batch. Base quenching was used before casting, while radiation quenching was applied during casting. The charge was discarded after magnesium treatment.

The samples were produced by Busch-Hungária Kft. in Győr, Hungary.



Figure 1. Photograph of a nodular cast iron test plate



Figure 2. LM image of the surface of the cast-iron test plate

2.1.2. Methods

The surface structure of the raw metals was visualized using a KEYENCE VHX-2000 series digital optical light microscope (LM) (Figures 2 and 3). The chemical composition of the raw metals was analyzed by a SPECTRO M8 spark and arc-excited optical emission spectrometer (OES) from Oxford Instruments.

The sample plate was remelted/recasted before being tested by converting it from graphite into carbide form. When a spark is produced, the graphite burns, creating a disturbance by sending false signals to the sensors and contaminating the glass window with smoke. When the specimen is remelted, the carbon is in the form of carbide, which is not burned by the spark, thereby yielding the desired excitation, moreover, the carbon is more evenly distributed. Since in this case it is important to completely remelt the sample and rapidly cool it, graphite is not reformed.

The samples are grinded with 60 grit sandpaper, inductively melted in a remelting furnace and quickly cooled to prevent the formation of graphite. These remelted samples were then ground again with 80 grit sandpaper before being dusted and tested. Three measurements were performed on each sample due to the inhomogeneity of the raw material.

The chemical composition used during OES (as weight %) of the cast-iron sample plate is presented in Table 1.

Table 1. Chemical composition of samples by OES

| | | | | |
|-------|--------|--------|---------|--------|
| C | Si | Mn | P | S |
| 3.66 | 2.276 | 0.31 | 0.023 | 0.005 |
| Cr | Mo | Ni | Al | Co |
| 0.04 | 0.01 | 0.02 | 0.0073 | <0.01 |
| Cu | Ti | Pb | Sn | Mg |
| 0.32 | 0.0149 | <0.02 | 0.005 | 0.0344 |
| Ce | Sb | B | N | Fe |
| 0.009 | 0.003 | 0.0006 | <0.0010 | 93.25 |

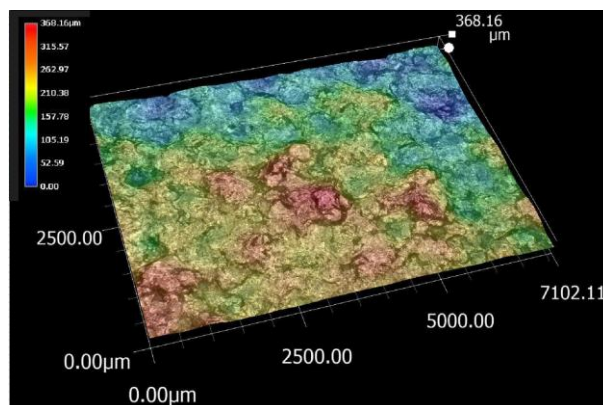


Figure 3. 3D LM image of the surface of the test plate

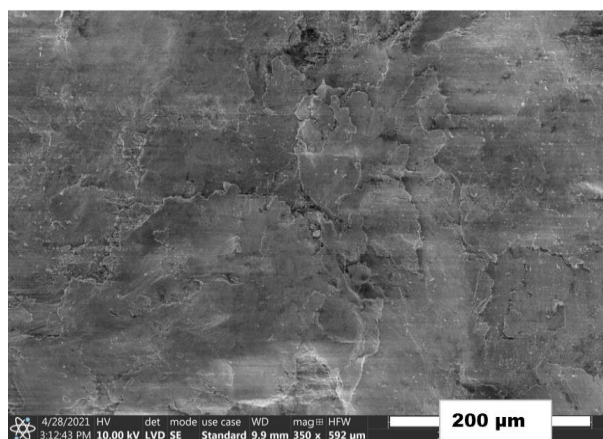


Figure 4. SEM image of the surface morphology of the cast-iron test plate

The morphology as well as the shape and size of the crystals were tested by a FEI/Thermo Fisher Scientific Apreo S LoVac scanning electron microscope (SEM). Observations by a SEM were made in the low vacuum mode with an acceleration voltage of 20.0 kV (Figure 4).

Table 2. Chemical composition of the samples (EDX)

| elements | C K | Al K | Si K | Mn K | Fe K |
|----------|------|------|------|------|-------|
| weight % | 3.14 | 0.12 | 1.93 | 0.39 | 58.49 |

The elemental compositions of the samples were determined by an EDAX AMETEK Octane Elect Plus Energy Dispersive X-ray Analyzer (EDX). The acceleration voltage was 20 kV and the data collection time period was 180 seconds.

The chemical composition (as weight %) of the cast-iron samples is displayed in Table 2.

Metallographic Analysis

The test plates were cut into pieces with a cutting saw before 4x4x4 cm cubes were cut out using a hand saw in order to carry out the metallographic analysis. Special attention was given to ensure the condition of the surfaces was good. The surface was ground in the first step using P120 and in the second with P400 grit sandpaper. It was then polished using NEODIA diamond abrasive solution; in the first step, a suspension solution formed from 9 μm particles was employed, while in the second step, a polishing machine (Struers RotoPol-22 with a rotation speed of 150 rpm) was used with grains 3 μm in diameter to smoothen and polish the surface. The sample was also subjected to chemical attack using 2 % Nital etchant for 10 seconds to highlight the microstructure of the matrix.

The micrographs were processed using a Nikon Eclipse ME600 optical microscope and the "a4iDOCU" computer program evaluated the images by conducting a metallographic examination, thereby providing the average values of the graphitic, ferritic and pearlitic fractions as well as the number and size of the graphite nodules.

Microstructure

Figure 5 shows the surface of the unetched sample in which the graphite are the black spots.

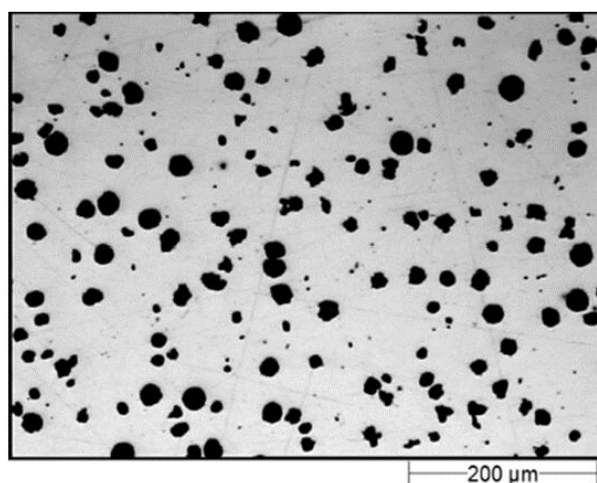


Figure 5. Micrograph of the spherical morphology of the graphite nodules of the nodular cast iron

It can be seen that the graphite spheres are fine, round and uniform in nature. According to DIN EN ISO 945, they are classified as size 6 with a graphite form of class V-VI, i.e. irregular and regular nodular-like graphite particles (reference images of the most common form of graphite according to Standard ISO 945-1:2017).

The surface following the etching process is shown in Figure 6 in which the ferrite appears white. Its microstructure consists of pearlite/ferrite phases and nodular graphite in the form of microscopic spheres of graphite, while its structure consists of a mixture of pearlite and ferrite, which is the most common matrix for commercial grades of ductile iron.



Figure 6. Microstructure of the matrix

Preparation of the zinc phosphate coating

The test plates were blasted with S390 (44 HRC) steel grit before zinc phosphating. The surface roughness was $R_z = 98 \mu\text{m}$, that is, the maximum height of the profile.

The blasted ductile-iron sample plates were pretreated together with other sample plates as well as pieces made of steel and aluminum alloys in the same technological step simultaneously under industrial conditions according to a previously published process and its parameters [30].

The samples were subjected to surface pretreatment and phosphating using a dipping process with a nitroguanidine or nitrite-based accelerator. After pretreatment, the samples were dried in a laboratory oven. Important parameters of phosphate baths are the free acid value (FA) which refers to the free H^+ ions present and the total acid value (TA) which represents the total phosphate content of the phosphate bath [8]. In our experiments, these parameters were as follows: FA=1.5 points; TA=22 points [30].

The samples were degreased, rinsed, activated, phosphated and rinsed again in successive steps using different baths. In the degreasing bath, any residual surface contamination was removed from the metal surface; in the rinsing bath(s), the degreasing chemicals were removed with water; in the subsequent bath, the metal surface was activated; in the phosphating bath, insoluble heavy-metal tertiary phosphates formed on the surface; and finally in the rinsing bath, acid residues, soluble salts and non-adhesive particles were removed from the metal surface [30].

Gardobond 2600 tricationic (Mn^{2+} , Zn^{2+} , Ni^{2+}) zinc phosphating solution (BASF, Chemetall Ltd.) was used for the experiments, which can be used for phosphating iron and steel by a dipping and spraying process. Although this is a nitrite (N)-accelerated system, according to the manufacturer's technical data sheet (TDS), it can also work with a nitroguanidine (NG) accelerator. For both series of experiments with the accelerators, a zinc-phosphating solution was used by applying the same settings and the accelerators were dosed at low (L), medium (M) and high (H) levels in accordance with the TDS. First, the samples were degreased with the Gardoclean S 5197 alkaline cleaner (BASF, Chemetall Ltd.). During the tests, the dipping method was employed with Gardobond Additive H7400 (BASF, Chemetall Ltd.) as the surfactant at 60 °C for 600 s by intensively mixing the bath. Having been rinsed with tap water, the surface was activated with Gardolene V6513 solution (BASF, Chemetall Ltd.) at a pH of 8.9. The zinc phosphating step was carried out using Gardobond 2600 solution (BASF, Chemetall Ltd.) at a temperature of 53 °C over an exposure time of 180 s. The bath used for both accelerators contained 1.3 g/L zinc and a 2.4 gas-point N accelerator measured by a gas burette or a 500 mg/L NG accelerator measured by photometry. After the phosphating process, the surface was rinsed with water over two steps. In order to remove any residual salt content from the surface, a cascade rinse system using deionized water was employed. Finally, the pretreated samples were air-dried [30]. The composition of the bath and labeling of the samples are shown in [Tables 3 and 4](#), respectively.

Cathodic Electrocoating

The zinc phosphated sample plates were painted using the cathodic dip coating (CED) process with the POWERCRON® P6200HE electrocoat (PPG Industrial Coatings France). The electrocoat consisted of DI (deionized water) 50.01 wt.%; CR693A resin 43.51 wt.% and CP471A pigment paste 6.48 wt.%, which was continuously mixed in the painting bath to ensure homogeneity. The temperature of the paint was maintained at the specified temperature by a cooling-heating system within the range of ± 1 °C. The solvent in the bath consisted of hexylene glycol (HG) and methoxy propanol (PM).

The parameters of the bath and the applications of electrodeposition are shown in [Tables 5 and 6](#), respectively.

Adhesion of the layer of paint was inspected by manual cross-cut testing according to the ISO 2409 standard. Six parallel cuts were applied using a template and an Elcometer 107 cross hatch cutter down to the underlying surface, the distance between which was 1 mm. Then six further cuts were made at right angles to each other, resulting in an even rectangular pattern. All loose particles close to where the cross cuts were made were removed with adhesive tape as specified by the standard. The test surface was then assessed by comparing it with images in the table from the standard.

Depending on their length, cross cuts ranging from 0 to 5 were made.

Table 3. Chemical composition of the phosphating baths

| Parameters | | Limits |
|-----------------------|-------------|----------------|
| Bath acidity (points) | Free acids | 1.5 |
| | Total acids | 22.0 |
| Tri-cations (g/L) | Zn^{2+} | 1.3 |
| | Ni^{2+} | 0.9 |
| | Mn^{2+} | 0.9 |
| F ⁻ (ppm) | | 140-150 |
| Accelerator | N-L | 1.4 gas points |
| | N-M | 2.4 gas points |
| | N-H | 3.8 gas points |
| | NG-L | 0.2 g/L |
| | NG-M | 0.5 g/L |
| | NG-H | 1.0 g/L |

Table 4. The symbols of samples

| accelerator: NG | | accelerator: N | |
|-----------------|-------|----------------|-----|
| low | NG- L | low | N-L |
| medium | NG-M | medium | N-M |
| high | NG-H | high | N-H |

Table 5. Analysis of the CED bath

| Test | Specifications | | Results |
|-------------------------------|----------------|------|---------|
| | min. | max. | |
| Solids for 1h at 110 °C (%) | 17 | 19 | 17.77 |
| Pigment to Binder ratio (P/B) | 0.15 | 0.17 | 0.161 |
| pH | 4.9 | 5.3 | 5.31 |
| Conductivity (μ S/cm) | 1200 | 1800 | 1621 |
| HG (%) | 0.1 | 0.4 | 0.3831 |
| PM (%) | 0.0 | 0.2 | 0.0913 |

Table 6. Parameters of the applications of electrodeposition

| Voltage | Temperature | Baking conditions | Thickness ISO 3882 |
|-----------|-----------------|---------------------------------|--------------------|
| 270 V | 34°C | 30 mins. (metal) at 165°C | ≈ 40 μm |
| Ramp time | Deposition time | Baking method | |
| 15 s | 120 s | Lab oven | |

The level of adhesion on each sample plate was GT0, namely the edges were completely smooth and none of the squares of the lattice detached.

Corrosion Resistance Test

The test plates were investigated after the coating had been completely cured in accordance with DIN EN ISO 9227-NSS after 504 hours; evaluation: DIN EN ISO 4628-1; surface corrosion: DIN EN ISO 4628-3; blistering: DIN EN ISO 4628-2 after 168/336/504 hours; delamination: DIN EN ISO 4628-8 after just 504 hours.

3. Results and Discussion

3.1. Coating morphology and analysis

Figure 7 shows that both accelerators create a uniform, thorough zinc phosphate layer on the surface of the spheroidal casting sample. When the nitrite-based accelerator was used (D-F), the crystals formed were larger but their growth was sometimes irregular in some areas. However, when a nitroguanidine accelerator was used (A-C), the structure of the crystalline layer was more uniform.

Compared with the SEM images published by Li et al. [8], it can be concluded that by applying the composition of the phosphating bath outlined in Table 3, it was possible to create a coating with a suitable structure without having to add sodium molybdate (Na_2MoO_4) or other additives.

Nejrenu et al. [21] showed in their work that the zinc phosphate coating created on the surface of the nodular cast iron substrate deposited by immersion contains acicular dendritic crystallites uniformly distributed over the entire surface with small gaps between them. No needle-like crystals were visible on the surface during our experiments and the coating was free of gaps.

The microstructure of the zinc phosphate coating on the ductile cast-iron surface and the structure of the zinc phosphate layer formed on the surface of the S420MC-grade steel during the same process (1-3) using the nitroguanidine accelerator are compared in Figure 8: It can be concluded that the uniform zinc phosphate layer on the steel surface was formed only when applying high accelerator dosages (Figure 8/3). A uniform, continuous

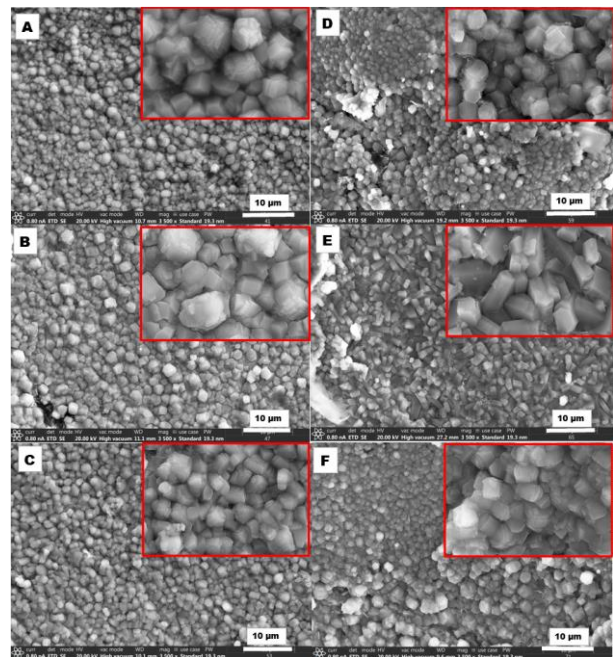


Figure 7. SEM micrographs of samples NG-L(A), NG-M(B) and NG-H(C) as well as N-L(D), N-M(E) and N-H(F)

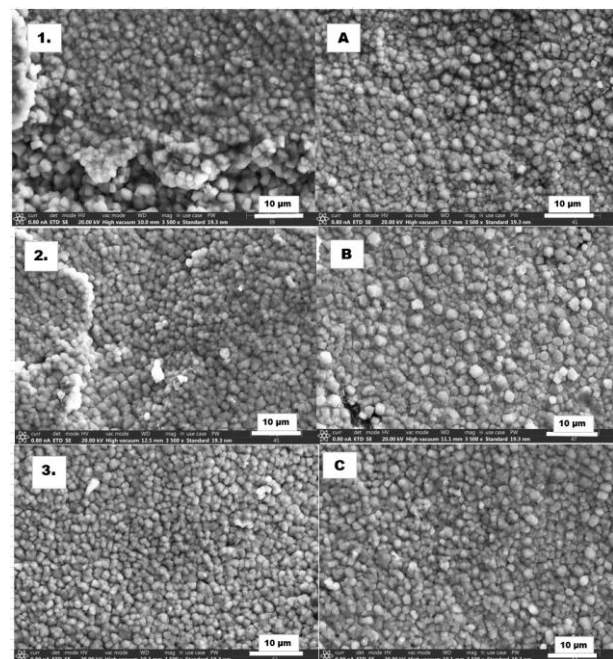


Figure 8. SEM micrographs of the zinc phosphate coating on S420MC steel (1-low; 2-normal; 3-high level nitroguanidine accelerator) and on the surface of samples NG-L(A), NG-M(B) and NG-H(C)

layer of zinc phosphate evenly covering the base metal was formed on the spheroidal cast iron (A-C), even when applying low accelerator dosages.

The microstructure of the zinc phosphate coating on the ductile cast iron surface is compared with the structure of the zinc phosphate layer formed on the surface of the S420MC-grade steel during the same

Table 7. EDX analysis of the zinc phosphate layer of the samples (wt.%)

| | NG-L | NG-M | NG-H | N-L | N-M | N-H |
|----|-------|-------|-------|-------|-------|-------|
| O | 24.72 | 22.74 | 26.18 | 25.60 | 28.40 | 25.28 |
| Al | 0.06 | 0.09 | 0.12 | 0.09 | 0.47 | 0.00 |
| Si | 1.29 | 1.42 | 1.24 | 1.57 | 1.93 | 1.91 |
| P | 7.48 | 7.69 | 7.78 | 7.45 | 8.38 | 7.61 |
| Mn | 1.50 | 1.51 | 1.73 | 1.57 | 1.56 | 1.45 |
| Fe | 53.58 | 54.66 | 50.30 | 51.16 | 47.42 | 52.70 |
| Ni | 0.39 | 0.30 | 0.56 | 0.36 | 0.24 | 0.18 |
| Zn | 10.98 | 11.59 | 12.09 | 12.20 | 11.61 | 10.87 |

process (4-6) by using the nitrite-based accelerator in *Figure 9*. It can be concluded that a uniform zinc phosphate layer on the steel surface formed only at low accelerator dosages (*Figure 9/4*) since irregular crystals were observed in the surface coating on the samples of spheroidal cast iron (D-F) when all three dosages were applied.

The EDX measurements of the zinc phosphate layers of the samples are presented in *Table 7*. It can be concluded that due to similarities between the measurements, zinc phosphate layers of similar compositions were formed on each sample, so neither substituting the accelerators nor altering their quantities had any effect on the composition of the layers formed on the surfaces.

3.2. Coating morphology and composition after the 504-hour-long Natural Salt Spray Test

The sample plates were rinsed with deionized water to remove the residues of sodium chloride solution off the surfaces. Once the corrosion evaluation had been completed, an SEM and EDX examination was performed on a 0.5 mm-wide scratch. The SEM measurements show that even after the 504-hour-long Natural Salt Spray Test, a zinc phosphate layer remained on the base metal as can be seen in *Figure 10*, which is confirmed by the EDX results presented in *Table 8* as both zinc and phosphorus are present in the corrosion scratch on the metal surface. The sodium and chloride seen in the measurement results are the remnants of the sodium chloride used during the corrosion test that remained on the surface of the samples after rinsing.

The origin of the copper in the measurements seen in *Table 8* can be attributed to cross-contamination from the corrosion chamber, since neither the base metal nor the phosphating solution contained copper.

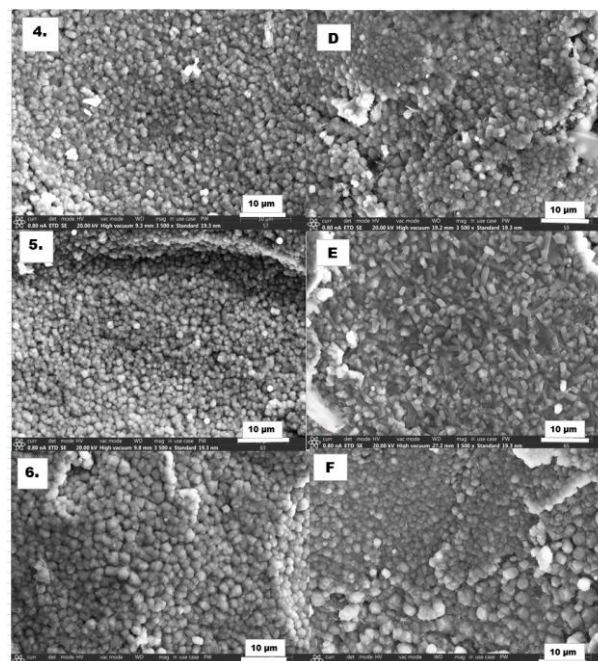


Figure 9. SEM micrographs of the zinc phosphate coating on S420MC-grade steel (4-low; 5-normal; 6-high nitrite-based accelerator dosage) and on the surfaces of the samples N-L(D), N-M(E) and N-H(F)

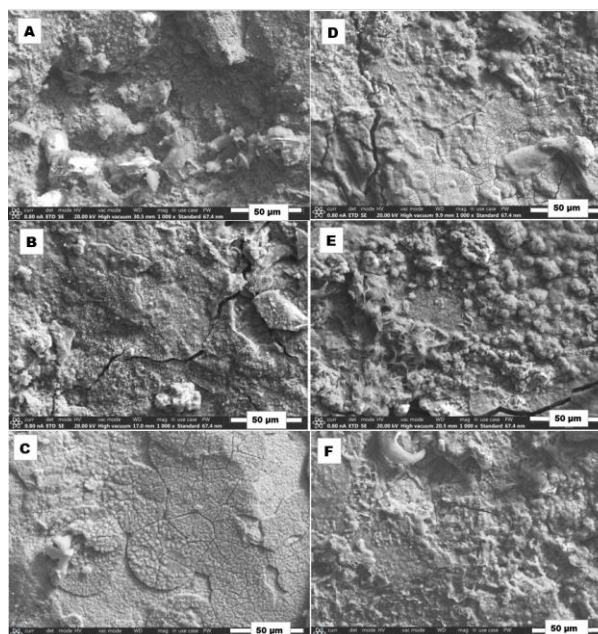


Figure 10. SEM micrographs of the corrosion residue after a 504-hour-long Natural Salt Spray Test on samples NG-L(A), NG-M(B), NG-H(C), N-L(D), N-M(E) and N-H(F)

3.3. Corrosion resistance test according to ISO 9227-NSS

The sample plates were tested according to ISO 9227-NSS and evaluated according to ISO 4628-1,2,3 after 168, 336 and 504 hours. This standard defines a method for determining the quantity and size of defects as well

Table 8. EDX analysis of the corrosion residue after a 504-hour-long Natural Salt Spray Test (wt.%).

| | NG-L | NG-M | NG-H | N-L | N-M | N-H |
|----|-------|-------|-------|-------|-------|-------|
| O | 40.27 | 36.55 | 35.55 | 37.68 | 37.88 | 33.66 |
| Na | 0.01 | 0.00 | 0.00 | 0.00 | 0.00 | 0.00 |
| Si | 2.13 | 4.46 | 3.36 | 4.11 | 3.27 | 2.22 |
| P | 1.42 | 0.51 | 0.93 | 0.40 | 0.06 | 0.80 |
| Cl | 2.60 | 3.74 | 4.41 | 2.87 | 5.06 | 3.09 |
| Mn | 0.27 | 0.28 | 0.35 | 0.22 | 0.40 | 0.44 |
| Fe | 51.62 | 53.39 | 52.59 | 53.49 | 51.89 | 57.93 |
| Ni | 0.09 | 0.02 | 0.08 | 0.18 | 0.15 | 0.14 |
| Cu | 0.27 | 0.68 | 0.55 | 0.76 | 1.03 | 0.49 |
| Zn | 1.33 | 0.36 | 0.76 | 0.28 | 0.26 | 1.22 |

as the degree of change in the appearances of the coatings, moreover, assesses the amount of rusting and blistering of the coatings by comparing them to standard reference images. Having been excluded from the evaluation, the cutting edges were not taken into consideration.

Immediately after the end of the testing period, the painted test panels were evaluated according to ISO 4628-8, which outlines a method for assessing delamination and corrosion around a scratch or other artificial defects on a coated panel.

Before the corrosion test, the thickness of the CED paint layer was measured according to the ISO 3882 standard with a "byko-test 8500" portable dry film thickness gauge (BYK-Gardner). Although the thickness of the paint layer was approximately 40 µm on all test plates, due to the high degree of surface roughness, the standard deviation of the measurements varied greatly, so their accuracy could not be guaranteed. An uncoated sample plate was used as a "zero plate" and the gauge calibrated to this plate.

The results of the corrosion tests presented in [Tables 9 and 10](#) show that neither the accelerator nor change in the dosage amount affected the corrosion resistance of the painted samples. Although vehicle manufacturers have different expectations regarding anti-corrosion coatings, these results meet their general expectations. According to [Table 10](#), no blisters formed on the paint layer of the samples, the degree of delamination was less than 1 mm, moreover, rust on the surface and cut edge corrosion did not occur on the surfaces treated in the phosphating bath containing the nitrite-based accelerator (Samples N-L, N-M & N-H). Among the samples treated in the phosphating baths containing the nitroguanidine accelerator presented in [Table 9](#), slight cut edge corrosion occurred even at low dosages, evidenced in Sample NG-L, as early as after 336 hours of testing. The effect of a medium dosage of

Table 9. Corrosion evaluation of samples treated with the nitroguanidine accelerator

| | | NG-L | NG-M | NG-H |
|-------|--|--------|--------|--------|
| 168 h | DIN EN ISO 4628-2 Blistering on surface | 0(S0) | 0(S0) | 0(S0) |
| | DIN EN ISO 4628-3 Rust on surface | Ri0 | Ri0 | Ri0 |
| | ISO 4628-1 Cut edge corrosion | KR0 | KR0 | KR0 |
| 336 h | DIN EN ISO 4628-2 Blistering on surface | 0(S0) | 0(S0) | 0(S0) |
| | DIN EN ISO 4628-3 Rust on surface | Ri0 | Ri0 | Ri0 |
| | ISO 4628-1 Cut edge corrosion | KR1 | KR0 | KR0 |
| 504 h | DIN EN ISO 4628-2 Blistering on surface | 0(S0) | 0(S0) | 0(S0) |
| | DIN EN ISO 4628-3 Rust on surface | Ri0 | Ri0 | Ri0 |
| | ISO 4628-1 Cut edge corrosion | KR1 | KR1 | KR0 |
| | DIN EN ISO 4628-8 Delamination | <0.5mm | <0.5mm | <0.5mm |

Table 10. Corrosion evaluation of samples treated with the nitrite-based accelerator

| | | N-L | N-M | N-H |
|-------|--|--------|--------|--------|
| 168 h | DIN EN ISO 4628-2 Blistering on surface | 0(S0) | 0(S0) | 0(S0) |
| | DIN EN ISO 4628-3 Rust on surface | Ri0 | Ri0 | Ri0 |
| | ISO 4628-1 Cut edge corrosion | KR0 | KR0 | KR0 |
| 336 h | DIN EN ISO 4628-2 Blistering on surface | 0(S0) | 0(S0) | 0(S0) |
| | DIN EN ISO 4628-3 Rust on surface | Ri0 | Ri0 | Ri0 |
| | ISO 4628-1 Cut edge corrosion | KR0 | KR0 | KR0 |
| 504 h | DIN EN ISO 4628-2 Blistering on surface | 0(S0) | 0(S0) | 0(S0) |
| | DIN EN ISO 4628-3 Rust on surface | Ri0 | Ri0 | Ri0 |
| | ISO 4628-1 Cut edge corrosion | KR0 | KR0 | KR0 |
| | DIN EN ISO 4628-8 Delamination | <0.5mm | <0.5mm | <0.9mm |

nitroguanidine was only evident at the end of the test period (NG-M). By applying a dosage exceeding the amount given on the technical data sheet as presented in [Table 3](#), the test results were identical to those of the test plates treated in the phosphating bath containing the nitrite-based accelerator (NG-H).

4. Conclusions

With the multimetal zinc phosphate baths used in these experiments, it was possible to form a uniform and fine

crystalline zinc phosphate layer on the surface of the steel plates without modifying the bath and by using nitrite-based (N) and nitroguanidine (NG) accelerators. The scanning electron micrographs did not show the different crystal structures of zinc phosphate crystals around the graphite spheres as described in the literature. No significant differences in the morphological properties of the zinc phosphate layers formed on the surfaces of the two base metals were observed by applying the same technological parameters. On the zinc phosphate conversion coating, the layer of electrophoretic paint adhered strongly (GT0) and no defects in the paint were observed. The 504-hour-long Natural Salt Spray Test, which is generally defined as the minimum requirement in the automotive industry, yielded satisfactory results when applying both accelerators. Since neither accelerator while operating at low, normal or high levels affected the corrosion resistance, it can be concluded that this zinc phosphate technology is robust and works well throughout the operating window, even beyond it, for ductile cast iron. Ductile cast iron can be treated in a similar way to steel surfaces when designing corrosion-resistant coatings. However, when treating steel and cast-iron surfaces together, it is preferable to use the softer nitroguanidine accelerator over a shorter reaction time instead of the nitrite-based one typically used for steels. To achieve the same effect as the nitrite-based accelerator, the dose rate should be increased.

Acknowledgements

The SEM studies were performed in the electron microscopy laboratory at the University of Pannonia and financed by grant no. GINOP-2.3.3-15-2016-0009 from the European Structural and Investments Funds as well as the Hungarian Government.

REFERENCES

- [1] Rausch, W.: Die Phosphatierung von Metallen - 3. Auflage (Leuze, E.G. Verlag KG, Bad Saulgau, Germany), 2005, ISBN: 9783874801973
- [2] Donofrio, J.: Zinc phosphating, *Met. Finish.*, 2000, **98**(6), 57–58, 60–73, DOI: 10.1016/S0026-0576(00)80392-X
- [3] Machu, W.: Nichtmetallische anorganische Überzüge (Springer-Verlag, Vienna, Austria), 1952, DOI: 10.1007/978-3-7091-5060-3
- [4] Bender, H.S.; Dale Cheever, G.; Wojtkowiak, J.J.: Zinc phosphate treatment of metals, *Prog. Org. Coat.*, 1980, **8**(3), 241–274, DOI: 10.1016/0300-9440(80)80018-X
- [5] Fettis, G.: Automotive paints and coatings (VCH Verlagsgesellschaft MbH, Weinheim, Germany), 1995, ISBN: 9783527286379
- [6] Sankara Narayan, T.S.N.: Surface pretreatment by phosphate conversion coatings - A review, *Rev. Adv. Mater. Sci.*, 2005, **9**(2), 130–177, https://www.ipme.ru/e-journals/RAMS/no_2905/narayanan.pdf
- [7] Sankara Narayan, T.S.N.: Phosphate conversion coatings – A metal pretreatment process, *Corros. Rev.*, 1994, **12**(3-4), 201–238, DOI: 10.1515/correv.1994.12.3-4.201
- [8] Li, G.-Y.; Lian, J.-S.; Niu, L.-Y.; Jiang, Z.-H.: A zinc and manganese phosphate coating on automobile iron castings, *ISIJ Int.*, 2005, **45**(9), 1326–1330, DOI: 10.2355/isijinternational.45.1326
- [9] Baloyi, T.; Maledi, N.; Andrews, A.: Corrosion performance of zinc phosphate coatings deposited on AA6061-HDG steel, *Mater. Chem. Phys.*, 2022, **283**, 126009, DOI: 10.1016/j.matchemphys.2022.126009
- [10] Thomer, K.W.: Materials and concepts in body construction, in: Automotive paints and coatings – Second edition, Streitberger, H.-J.; Dössel, K.-F. (Eds.), (Wiley-VCH Verlag GmbH & Co. KGaA, Weinheim), 2008, pp. 13–60, DOI: 10.1002/9783527622375.ch2
- [11] Todor, M.-P.; Kiss, I.: Systematic approach on materials selection in the automotive industry for making vehicles lighter, safer and more fuel-efficient, *Appl. Eng. Lett.*, 2016, **1**(4), 91–97, <https://aeletters.com/wp-content/uploads/2017/02/AEL00016.pdf>
- [12] Jhaveri, K.; Lewis, G.M.; Sullivan, J.L.; Keoleian, G.A.: Life cycle assessment of thin-wall ductile cast iron for automotive lightweighting applications, *Sustain. Mater. Technol.*, 2018, **15**, 1–8, DOI: 10.1016/j.susmat.2018.01.002
- [13] Fraš, E.; Górný, M.; Kapturkiewicz, W.: Thin wall ductile iron castings: Technological aspects, *Arch. Foundry Eng.*, 2013, **13**(1), 23–28, DOI: 10.2478/afe-2013-0005
- [14] Fraš, E.; Górný, M.; Lopez, H.: Thin wall ductile iron castings as substitutes for aluminum alloy casings, *Arch. Metall. Mater.*, 2014, **59**(2), 459–465, DOI: 10.2478/amm-2014-0076
- [15] Labrecque, C.; Gagné, M.; Javaid, A.; Sahoo, M.: Production and properties of thin-wall ductile iron castings, *Int. J. Cast Met. Res.*, 2003, **16**(1-3), 313–317, DOI: 10.1080/13640461.2003.11819601
- [16] Keough, J.R.; Hayrynen, K.L.: Automotive applications of austempered ductile iron (ADI): A critical review, *SAE Tech. Pap.*, 2000, DOI: 10.4271/2000-01-0764
- [17] Hack, M.; Jung, D.; Egner-Walter, A.: Optimized analysis process for the fatigue analysis of cast iron structures taking into account the local material structure, *Mater. Test.*, 2012, **54**(7-8), 497–502, DOI: 10.3139/120.110356
- [18] Gomes, O.D.F.M.; Paciornik, S.: Automatic classification of graphite in cast iron, *Microsc. Microanal.*, 2005, **11**(4), 363–371, DOI: 10.1017/S1431927605050415
- [19] Li, N.; Xing, S.-M.; Bao, P.-W.: Microstructure and mechanical properties of nodular cast iron produced by melted metal die forging process, *J. Iron Steel Res. Int.*, 2013, **20**(6), 58–62, DOI: 10.1016/S1006-706X(13)60112-0
- [20] Fragassa, C.: Investigating the material properties of nodular cast iron from a data mining perspective, *Metals*, 2022, **12**(9), 1493, DOI: 10.3390/met12091493

- [21] Nejneru, C.; Burduhos-Nergis, D.-P.; Axinte, M.; Perju, M.C.; Bejinarui, C.: Analysis of the physical-mechanical properties of the zinc phosphate layer deposited on a nodular cast iron substrate, *Coatings*, 2022, **12**(10), 1384, DOI: [10.3390/coatings12101384](https://doi.org/10.3390/coatings12101384)
- [22] Díaz, B.; Freire, L.; Mojio, M.; Nóvoa, X.R.: Effect of carbon on the corrosion and wear performance of Zn-phosphate layers, *Electrochim. Acta*, 2016, **202**, 299–309, DOI: [10.1016/j.electacta.2015.12.083](https://doi.org/10.1016/j.electacta.2015.12.083)
- [23] Gehmecker, H.: Pretreatment of multimetal car bodies, in: Automotive paints and coatings - Second edition, Streitberger, H.-J.; Dössel, K.-F. (Eds.), (Wiley-VCH Verlag GmbH & Co. KGaA, Weinheim), 2008, pp. 61–87, DOI: [10.1002/9783527622375.ch3](https://doi.org/10.1002/9783527622375.ch3)
- [24] Streitberger, H.-J.: Electrodeposition coatings, in: Automotive paints and coatings - Second edition, Streitberger, H.-J.; Dössel, K.-F. (Eds.), (Wiley-VCH Verlag GmbH & Co. KGaA, Weinheim), 2008, pp. 89–127, DOI: [10.1002/9783527622375.ch4](https://doi.org/10.1002/9783527622375.ch4)
- [25] Brüggemann, M.; Rach, A.: Electrocoat: formulation and technology (Vincentz Network, Hanover, Germany), 2020, pp. 80–81, DOI: [10.1515/9783748601074](https://doi.org/10.1515/9783748601074)
- [26] Tamilselvi, M.; Kamaraj, P.; Arthanareeswari, M.; Devikala, S.; Arockia Selvi, J.: Progress in zinc phosphate conversion coatings: A review, *Int. J. Adv. Chem. Sci. Appl. (IJACSA)*, 2015, **3**(1), 25–41, http://www.irdindia.in/journal_ijacsa/pdf/vol3_iss1/5.pdf
- [27] Benchadli, A.; Attar, T.; Messaoudi, B.; Choukchou-Braham, E.: Polyvinylpyrrolidone as a corrosion inhibitor for carbon steel in a perchloric acid solution: Effect of structural size. *Hung. J. Ind. Chem.*, 2021, **49**(1), 59–69, DOI: [10.33927/hjic-2021-08](https://doi.org/10.33927/hjic-2021-08)
- [28] Davis, J.R.: ASM Specialty Handbook Cast Irons (ASM International) 1996, pp. 54–79, ISBN: [9780871705648](https://www.isbn-international.org/product/9780871705648)
- [29] Davis, J.R.: ASM Specialty Handbook Cast Irons (ASM International), 1996, pp. 140–146, ISBN: [9780871705648](https://www.isbn-international.org/product/9780871705648)
- [30] Herbáth, B.; Kovács, K.; Jakab, M.; Makó, É.: Crystal structure and properties of zinc phosphate layers on aluminum and steel alloy surfaces, *Crystals*, 2023, **13**(3), 369, DOI: [10.3390/cryst13_030369](https://doi.org/10.3390/cryst13_030369)